Tellus (1982), *34*, 293–306

A steady state model for buoyant surface plume hydrodynamics in coastal waters

By RICHARD W. GARVINE, *College of Marine Studies, University of Delaware, Newark, DE 19711, U.S.A.*

(Manuscript received March 20; in final form July 14, 1981)

ABSTRACT

Shallow, surface plumes of buoyant water are frequently discharged into coastal waters by rivers, bays, power plants, and other sources. The most readily observed portion of these plumes is the near field where the initial expansion of plume water occurs, and where there is large contrast between plume and ambient water. In contrast to existing turbulent jet models of such plumes, the present model divides the plume near field into two domains, a frontal domain where turbulent exchange between plume and ambient water is intense, and the remainder of the flow where the dynamics of inviscid, nonlinear gravitational spreading of a shallow buoyant layer dominates. Using this approach, the steady state flow produced by the supercritical outflow of buoyant water from a channel at a coast into ambient water with a uniform alongshore current is modelled. Earth rotation is neglected. Frontal jump conditions developed in an earlier paper are applied to match the flow at the frontal boundary with the remainder of the plume. Numerical solutions for the entire flow are found by the method of characteristics, but much of the flow can be determined by simpler analytic computation. The computed flow fields show that a frontal boundary forms on the upstream or offshore side of the plume where the oncoming ambient current contains the gravitational spreading of the buoyant water. No front forms on the corresponding downstream, inshore side. In the body of the plume the flow simultaneously expands and turns downstream toward alignment with the ambient current. Relatively little change in plume water speed occurs, but the pressure field required for turning the flow downstream results in deepening of the plume interface offshore near the front. This, in turn, concentrates plume volume flux along its offshore side near the front. The maximum angle through which the flow may be turned initially is less than 66°. Outlet channel angles greater than this produce plumes which are separated from the shoreline by ambient water. The model results explain many of the observed features of the Connecticut River plume in Long Island Sound.

1. Introduction

Surface plumes of buoyant water are common features of coastal and inland waters. There are a variety of known mechanisms that generate them, such as the discharge of fresh or brackish water by rivers, estuaries, or bays into coastal seawater and the discharge of heated water from power plants into lakes, rivers, or the ocean.

It is useful to divide buoyant surface plumes into three contiguous spacial fields, here termed the source, near, and far fields. The source field is that in the immediate vicinity of the source of buoyant water, such as the mouth of a river. The near field is where the initial expansion of plume water occurs and where the contrast between plume and ambient water is still large. Usually its outer boundary is marked by a sharp frontal region. Beyond lies the far field where the final blending of source water with the ambient water occurs.

Fig. 1 shows the configuration of a river plume near field, the Connecticut River plume in Long Island Sound, for the period just after flood tide. A frontal boundary forms the offshore (eastern) edge of the plume, the upstream side along which the flood (westward moving) tidal currents had been

0040-2826/82/030293-14$02.50/0

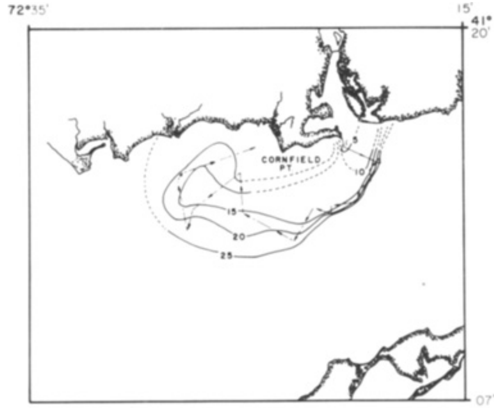

Fig. 1. Isohalines in p.p.t. at 0.5 m depth for the Connecticut River plume in Long Island Sound after flood tide. The line with arrows marks the ship track. North is toward the top. From Garvine (1974a).

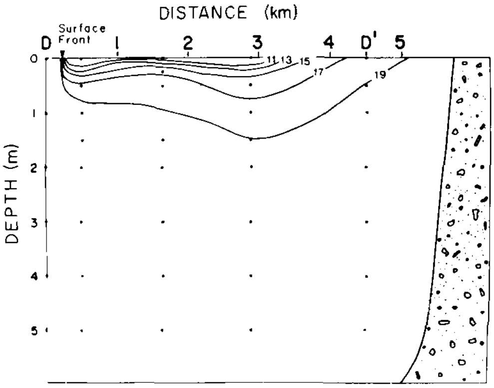

Fig. 2. Vertical section of density (sigma-t) across the Connecticut River plume during ebb tide, from Garvine (1977).

impinging. The body of the plume is about 15 km long and 7 km wide. Fig. 2 shows a vertical cross-section of the plume density (σ_t) field obtained on a different day and during ebb tide. Plume water has a much lower σ_t than the coastal seawater. The very shallow nature of the plume is clear, the plume depth to breadth ratio being only about 10^{-4}. The plume is also shallow compared to typical water depths, roughly one meter compared to thirty. Again a front forms the offshore, upstream boundary, now the western side where the eastward moving tidal currents were impinging. No front is found inshore, however.

In the near field of buoyant plumes the flow dynamics is dominated by gravitational spreading of the thin layer of buoyant fluid over the heavier ambient fluid. The leading edge of the spreading motion is a frontal region where the horizontal property gradients are largest and where turbulent exchange is concentrated (Garvine and Monk, 1974; Garvine, 1974b; Kao et al., 1977). For river plumes the horizontal extent of the frontal region is about 100 m. Over the remainder of the near field properties change slowly in space and the vertical stratification is very high. The near field has thus two disparate horizontal length scales, the frontal zone scale and the scale of the near field as a whole.

Most buoyant surface near field models have a conceptual basis in the dynamics of a turbulent jet discharging into ambient water. A review of representative models is given in Garvine (1981). In the present paper a different modelling approach is used that partitions the upper layer flow field into two domains, a frontal domain where dissipative effects are concentrated and horizontal gradients are very high, and the remainder of the near field where they are low. Hereafter these two domains are called the front and the plume body, respectively. The model treats the front as a moving discontinuity across which flow properties are related by appropriate jump conditions. The flow in the plume body is determined by using the nonlinear, long, internal wave equations for a shallow upper layer whose solutions are found subject to matching with the jump conditions at the front. This approach is not new, but has been used extensively for the treatment of the analogous problem of shallow, homogeneous single layer flows which include bores or hydraulic jumps (Stoker, 1957, Chap. 10) as well as for two-layer flows of simple geometry (Abbott, 1961).

A fundamental part of the approach then is the application of appropriate jump conditions at the front. These conditions incorporate the important effects of turbulent mass and momentum exchange across the plume interface in the frontal zone with the ambient fluid below; they may be viewed as extensions of the classical bore jump conditions (Stoker, 1957, Chap. 10). I recently derived these jump conditions (Garvine, 1981) for application to shallow, buoyant layer fronts of small enough scale, such as river plume fronts, that Coriolis effects are negligible.

In this paper I use the above approach to solve the horizontally two-dimensional, steady flow problem posed by the discharge of a shallow layer of buoyant fluid from an outlet channel at a coast into an unbounded domain of ambient water having uniform alongshore motion (Fig. 3a). An ambient current is a necessary condition for a steady state, since in its absence time dependent spreading of the buoyant layer would continue indefinitely. This problem thus includes the basic features of horizontal gravitational spreading, frontal boundaries, and an ambient current.

2. Governing equations for the plume body

Fig. 3b illustrates the model geometry in a vertical, offshore section through the plume. The

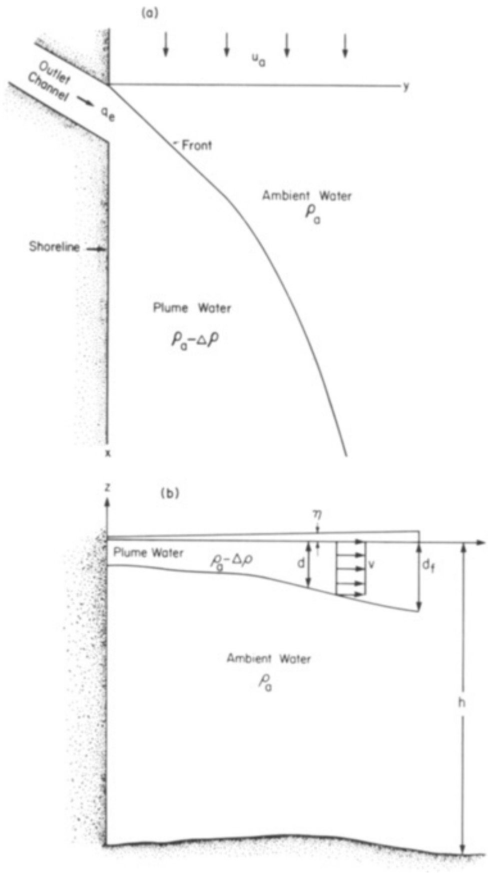

Fig. 3. Schematic of model geometry. (a) Plan view. (b) Vertical, offshore section.

alongshore, offshore, and vertical coordinates are x, y, z, respectively. The flow is assumed steady in these coordinates. The local depth of plume water is d, everywhere small compared to the local water depth h. The ambient water density is uniform at ρ_a, while the plume water density is uniform at $\rho_a - \Delta\rho$. At the offshore boundary of the plume the front is shown as a discontinuity with plume depth d_f shoreward of the front. The local free surface elevation above ambient level is η. Wind stress is neglected. The motion is assumed to be inviscid everywhere but at the front. The plume is restricted to sufficiently small scales that Coriolis effects are negligible. The vertical momentum balance is assumed to be hydrostatic. Since $\Delta\rho/\rho_a$ is small for all plumes of interest, the Boussinesq approximation will be invoked. Thus, the plume will be floating in isostatic balance upon the ambient water. Consequently, η and d are simply related by $\eta = (\Delta\rho/\rho_a)d$ + constant, and the horizontal pressure gradient within plume water is simply given by $\nabla p/\rho_a = g'\nabla d$ where ∇ is the horizontal gradient operator and $g' \equiv g\Delta\rho/\rho_a$, the reduced gravity. Since g' is uniform, ∇p in the plume varies only with the interface slope, ∇d. The horizontal fluid velocity vector $\mathbf{q}$ *in the plume is then vertically* uniform, as indicated in Fig. 3b.

The continuity and horizontal momentum equations of the plume body consistent with these restrictions may be written in vector form as,

$$\nabla \cdot (d\mathbf{q}) = 0 \tag{1}$$

$$(\mathbf{q} \cdot \nabla)\mathbf{q} + g'\nabla d = 0 \tag{2}$$

For this model it will be more convenient to replace (2) by the equivalent expressions for the conservation of potential vorticity and mechanical energy (or Bernoulli equation) along the streamlines.

$$(\mathbf{q} \cdot \nabla)(\zeta/d) = 0 \tag{3}$$

$$(\mathbf{q} \cdot \nabla)\left(\frac{q^2}{2} + c^2\right) = 0 \tag{4}$$

where ζ is the vertical component of vorticity, $q \equiv |\mathbf{q}|$, the fluid speed, and c the internal wave phase speed given by $c^2 = g'd$. I introduce now a further restriction which permits considerable simplification of (3) and (4) without sacrificing any fundamental physical property. The source field flow state within the outlet channel is assumed to be horizontally uniform; thus, $\zeta = 0$ there for all streamlines. Consequently, by (3) the flow remains irrotational throughout the plume body. The mechanical energy, $q^2/2 + c^2$, will also be uniform within the outlet channel; therefore, by (4) it will remain so throughout the plume body. Thus the integral of (4) is simply,

$$\frac{q^2}{2} + c^2 = c_0^2 \tag{5}$$

with c_0 a constant equal to the phase speed for stagnant fluid.

The system of (1) and (5) together with $\zeta = 0$ has the same form as the equations governing the two-dimensional, steady potential flow of a compressible fluid whose density is the analog to d here. Consequently, the plume flow problem, as posed, may be solved by the same methods used in compressible, potential flow problems. A similar compressible flow analogy for two-dimensional stratified flow has also been formulated by Jirka (1980). Stronach (1981) has developed a more complicated model for application to the Fraser River plume which includes interfacial friction and mass entrainment throughout the plume body. As in compressible flows, the local ratio of fluid speed to wave speed is a variable of major importance. Here this ratio is given by the internal Froude number $F \equiv q/c$. The flow for $F < 1$, $F = 1$, and $F > 1$ is termed subcritical, critical, and supercritical, respectively. Hereafter I will restrict all flows in the outlet channel and beyond to be supercritical. This is consistent with outlet conditions for most power plant discharges as well as with observations of the Connecticut River at its mouth (Garvine, 1974a) and within its plume (Garvine, 1977). Uniformly supercritical flows are much simpler to compute, since their governing equations are hyperbolic.

Following Ferri (1954), the two characteristic lines passing through a given point have the slopes,

$$(\mathrm{d}y/\mathrm{d}x)_+ = \tan(\theta + \phi) \tag{6a}$$

$$(\mathrm{d}y/\mathrm{d}x)_- = \tan(\theta - \phi) \tag{6b}$$

where θ is the local angle made by $\mathbf{q}$ with the x-axis and ϕ is the Froude angle (analogous to the Mach angle) given by

$$\phi = \sin^{-1}(F^{-1}) \tag{6c}$$

As in compressible, supersonic steady flow, the two characteristic lines form the loci of the wave fronts, here the long internal wave fronts, inclined at angle ϕ to each side of the local streamline. From (6c) ϕ is bounded by 0 ($F \to \infty$) and 90° ($F = 1$, or critical flow). A collection of characteristic lines in a neighborhood given by (6a) will be termed a plus family, while those given by (6b) will be termed a minus family.

Along the characteristic lines changes in q and θ are related by the corresponding characteristic equation,

$$\mathrm{d}q = \pm q \tan\theta \,\mathrm{d}\theta \tag{7}$$

where the equation with the plus sign is applicable to (6a) and the minus sign to (6b). The two equations of (7) together with (5) constitute the system of governing equations for the plume body. They may be solved for the dependent variables, q, θ, and c, once θ and q or c have been specified along a curve upstream which is nowhere parallel to a characteristic line. For the present model this will be done by a simple finite difference method with the upstream conditions determined by the flow in the outlet channel.

Several physical features of the plume flow may be deduced without solving the system in detail. Equation (5) shows that there is a maximum fluid speed q_m corresponding to ultimate expansion of the fluid (c and hence d equal zero). From (5) this speed is simply

$$q_m = 2^{1/2} c_0 \tag{8}$$

By combining this with the definition of F, (5) may be rewritten as

$$(q/q_m)^2 = (1 + 2F^{-2})^{-1} \tag{9}$$

Thus, if q^* denotes the speed for critical flow ($F = 1$), we find

$$q^* = 3^{-1/2} q_m = (2/3)^{1/2} c_0 \tag{10}$$

For defining normalized variables, q^* is the most convenient of these speeds. The following normalized variables are thus introduced.

$$Q \equiv q/q^*, \quad C \equiv c/c^*, \quad D \equiv d/d^*$$

Here $(\ )^*$ denotes a variable corresponding to critical flow; thus, $c^* = q^*$, while $d^* = q^{*2}/g'$. Using the normalized variables, the equation of mechanical energy (5) may be rewritten

$$C = (3 - Q^2)^{1/2}/2^{1/2} \tag{11}$$

Thus,

$$D = C^2 = (3 - Q^2)/2 \tag{12}$$

and

$$F = Q/C = 2^{1/2}Q(3 - Q^2)^{-1/2} \tag{13}$$

Since the plume flow is restricted to be supercritical everywhere, we have $1 < F < \infty$, $1 < Q < 3^{1/2}$, $0 < C < 1$, and $0 < D < 1$.

3. Boundary conditions at the front

Fig. 4a shows the local frontal geometry at the plume boundary in a horizontal plane. Locally the front makes an angle α with the x-direction (alongshore). The plume water velocity just inside the front is $\mathbf{q}_f$ at angle θ_f. (Hereafter, "f" subscripts will denote properties just inside the front.) The ambient water has a uniform velocity $u_a\,\mathbf{i}$, where $\mathbf{i}$ is a unit vector alongshore. The coordinate locally normal to the front is $\bar{x}$.

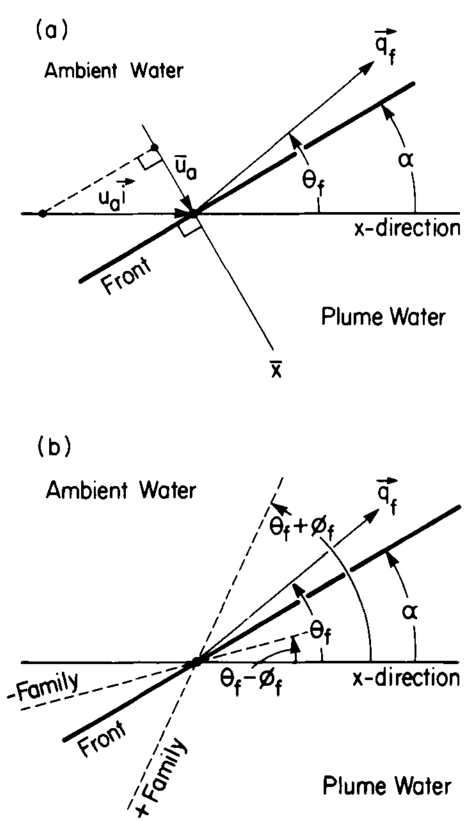

Fig. 4. Geometry at the plume frontal boundary in the horizontal plane. (a) Orientation of the local normal coordinate $\bar{x}$. (b) Geometry of the characteristic lines.

The frontal jump conditions were derived (Garvine, 1981) within the $\bar{x}$ coordinate system. These, when specialized to the present case of a vanishing upper layer on the upstream (ambient water) side give

$$\bar{u}_f = S_e \beta \bar{u}_a \tag{14}$$

$$c_f/\bar{u}_a \equiv 1/F_{a1} = [2\beta(S_e + \bar{d} - \beta)]^{1/2} \tag{15}$$

Here $\bar{u}$ is a velocity component measured along $\bar{x}$. S_e indicates the sign of the entrainment velocity in the frontal zone ($S_e = -1$ for downward and $+1$ for upward entrainment). For downward entrainment $\bar{u}_f < 0$ so that the flow behind the front is toward the front (convergent), while for upward entrainment the opposite is true. β is a positive, dimensionless constant which indicates the fraction of the frontal zone over which significant turbulent mass exchange (entrainment) and momentum exchange (interfacial friction and entrainment of momentum) occur; hence, the limit for vanishing exchange corresponds to $\beta \to 0$. The positive constant $\bar{d}$ specifies the ratio of the interfacial friction and entrainment coefficients, a quantity of order one.

The derivation of the frontal jump conditions, upon which (14) and (15) are based, was conducted for fronts across which there was no shear of the velocity locally parallel to the front between ambient and upper layer water. In the present application there will generally be some shear. Its effect will be to modify the bulk shear velocity across the interface in the frontal zone from the level $\bar{u}_a$ that is implicit in (14) and (15) to one somewhat higher. While this effect can be roughly accounted for, the degree to which the jump conditions are then changed is less than the change connected with the present uncertainty in appropriate values for β and $\bar{d}$. Consequently, this effect will be ignored here.

As discussed in Garvine (1981), there is a variety of evidence indicating that the frontal propagation Froude number $F_{a1} \equiv \bar{u}_a/c_f$ is close to unity for a variety of flow conditions. Since there is little experimental basis as yet for selecting a particular value for $\bar{d}$, I will instead set $F_{a1} = 1$ henceforth and treat β as a variable parameter. β

will influence $\bar{u}_f$ through (14) and, in effect, will determine $\tilde{d}$ through (15). For some cases I will force turbulent mass exchange to vanish by setting $S_e = 0$ (whence $\bar{u}_f = 0$ by (14)). Turbulent exchange will then be limited to interfacial friction.

To translate (14) and (15) into properties of the fixed coordinates, one must make the substitutions $\bar{u}_a = u_a \sin \alpha$ and $\bar{u}_f = -q_f \sin(\theta_f - \alpha)$, which follow from the geometry of Fig. 4a. Then, (14) and (15) become

$$-Q_f \sin(\theta_f - \alpha) = S_e \beta U_a \sin \alpha \tag{16}$$

$$C_f = U_a \sin \alpha / F_{a1} \tag{17}$$

where $U_a \equiv u_a/q^*$. Note that for downward entrainment ($S_e = -1$), $\theta_f > \alpha$ from (16), consistent with convergence, and the reverse for upward entrainment. If $F_{a1} = 1$, then (17) may be rewritten as $U_a/C_f = u_a/c_f = \csc \alpha \geq 1$; thus, a local steady state requires that the ambient velocity be at critical or supercritical speed with respect to the local phase speed inside the front.

The expressions (16) and (17), together with (11) applied at the front, provide three independent constraints on the four local frontal variables Q_f, θ_f, C_f, and α. A fourth constraint is needed to close the system. For the uniform flow region just beyond the outlet channel, one simply equates θ_f to the given outlet flow angle. For a point farther downstream, the fourth constraint arises from the characteristic equation (7) of the plus family which links the flow state at the front to the flow state upstream *within* the plume (Fig. 4b). Thus, a requirement for unique determination of the flow at the front is that the plus family characteristic have a local inclination greater than the front, i.e., $\theta_f + \phi_f > \alpha$. One may show, using (13) and (14), that this is satisfied if

$$\beta F_{a1} < 1 \tag{18}$$

In the computations where $F_{a1} = 1$ throughout, (18) requires only $\beta < 1$. As discussed in Garvine (1981), $\beta = 1$ is the largest value one could expect, based on analysis of the frontal zone dynamics.

4. Initial flow expansion

Fig. 5 shows the essentials of the plume geometry. The flow exits the outlet channel at inclination θ_e and speed Q_e and flows into a semi-infinite domain of ambient water. The outlet

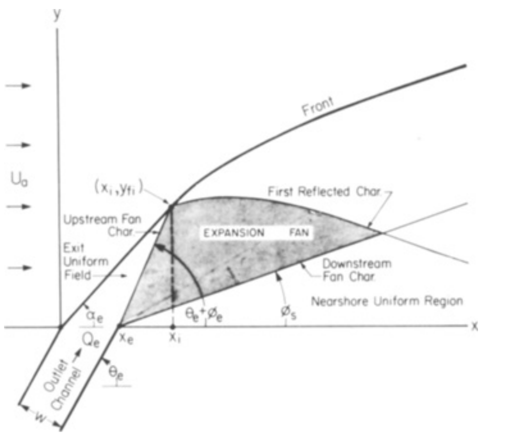

Fig. 5. Schematic of the model plume geometry. The x-axis lies along the shoreline.

channel width w is the single imposed problem length scale; consequently, the x and y coordinates are henceforth understood to be normalized by it. The corners formed by the intersections of the channel and the shoreline are taken as sharp for simplicity. The ambient water has simple uniform velocity along shore, U_a.

A variety of flow regions appear in Fig. 5. One may infer their existence and general characteristics from analogous compressible flow field geometries given in the literature, e.g., Ferri (1954).

As the flow exits the outlet channel it passes first through a triangular region of uniform flow where its properties are identical to those in the outlet channel. This region is thus termed the exit uniform field and is merely an extension of the outlet channel into the near field. Thereafter the flow passes into another triangular region. Here a train of waves is transmitted outward from the downstream corner of the outlet channel ($x = x_e$) signaling to the plume flow the increased horizontal area available. As the flow traverses this region it expands, while the streamlines spread apart horizontally, the fluid gains speed, the streamlines turn toward alignment with the shoreline and ambient current, and the pressure (at fixed z) falls as D and η decrease. These waves produce the basic horizontal expansion or gravitational spreading of the plume; hence, they will be termed expansion waves. Since in this region these waves fan outward from the downstream corner, this region is termed the expansion fan, a term also used in compressible flow dynamics. The waves in the expansion fan begin, and for some streamlines nearly complete, the expansion process. The offshore boundary of this region is set by the locus of the first characteristic reflected off the front. Fig. 5 shows these regions and other flow field properties in the x, y plane. In most plume fields a second triangular region of uniform flow, termed the nearshore uniform field, will exist bounded by the shoreline, the expansion fan, and the first reflected characteristic. The greater portion of flow changes, that is, the bulk of the plume expansion, will occur within the expansion fan. All three of these regions have sufficiently simple dynamics that they permit analytic calculation of their flow properties. For many applications these regions will contain most of the plume flow of interest. Then, the numerical computations by finite difference methods required to determine the flow state yet farther downstream may be spared.

The flow properties of the exit uniform field are the same as those of the outlet channel but with the added property of the frontal boundary. Since the properties are uniform, all streamlines are straight and inclined at θ_e, the angle of the outlet channel. The frontal boundary that forms the upstream boundary of this region must then also be straight and must terminate at the upstream channel corner ($x = 0$, $y = 0$) with an inclination α_e which is compatible with the other flow properties.

An outlet property of particular significance is the buoyant water volume flux $V_e \equiv q_e d_e w$. Using the normalized variables, it may be written

$$V_e = (wq^{*3}/g')(3 - Q_e^2)Q_e/2 \tag{19}$$

This shows clearly the dependence on q^*, and hence c_0. As the outlet channel flow Froude number becomes large, $3-Q_e^2$ approaches zero, and the volume flux vanishes. For zero mass entrainment in the frontal zone ($S_e = 0$), the plume volume flux will remain at V_e, for downward entrainment ($S_e = -1$) it will fall continually below V_e, and for upward entrainment ($S_e = +1$) it will increase above V_e.

Two limiting cases for the exit uniform field are of particular physical interest: large and small values of U_a. For large values the ambient longshore current is much more powerful than the outflow. From (17), then, it follows that $\sin \alpha_e \simeq \alpha_e \sim U_a^{-1} \ll 1$. Thus, as one might expect, the ambient current strongly confines plume spreading so that the frontal inclination is small and the front nearly seals off the outlet.

For the opposite limit, vanishing U_a, there is no mechanism to contain the spreading of the buoyant layer within a stationary domain. This is simply reflected by (17), which for this limit gives $C_e \to 0$. Consequently, $Q_e \to 3^{1/2}$ and $F_e \to \infty$. From (16) $\alpha_e \to \theta_e$, indicating that the outflow continues into the ambient domain without deflecting or spreading. However, (19) shows that V_e vanishes, underscoring the degenerate nature of this limit. Figuratively, when U_a vanishes, only a wisp of the buoyant discharge can survive in the steady state. Its shape then is a straight extension of width w of the outlet channel flow into the ambient domain.

If one specifies zero entrainment at the front ($S_e = 0$) the exit uniform field determination is particularly simple. The front then corresponds to a contact discontinuity and $\alpha_e = \theta_e$ by (16).

Determination of the flow field in the expansion fan is straightforward for two reasons. First, it is a region where only one family of characteristics, the plus family, contributes to flow changes. Such a region is termed a single family or simple wave region in compressible flows (Courant and Freidrichs, 1976, Chap. 3). Second, these plus family waves are centered at the corner $x = x_e$, i.e., they all originate there and fan outward. As a direct result of these two features, an analytic solution for the region exists. It is based on the Prandtl–Meyer relation valid for single family regions (Liepmann and Roshko, 1957, p. 99). For expansion waves this relation becomes in present variables

$$\theta + \nu(Q) = \theta_e + \nu(Q_e) \tag{20a}$$

where ν is the Prandtl–Meyer function

$$\nu \equiv 3^{1/2} \tan^{-1} \sigma - \tan^{-1} (3^{1/2} \sigma) \tag{20b}$$

with $\sigma(Q) \equiv [(Q^2 - 1)/(3 - Q^2)]^{1/2}$. ν increases monotonically from zero when $Q = 1$ (critical flow) to a maximum of $\nu_{max} = (3^{1/2} - 1)\pi/2 \simeq 66°$ for fully expanded flow ($Q = 3^{1/2}$ or σ and $F \to \infty$).

An immediate result of physical significance from (20) is that the maximum decrease in flow inclination angle θ through the expansion fan is ν_{max}. Thus, in the spreading process through the expansion fan the limiting minimum downstream flow angle is $\theta_e - \nu_{max}$, and this only if $F_e = 1$; otherwise the decrease is even less and the minimum angle greater. This limit reflects the fact that in passing through a single wave family the flow streamlines may be spread or opened up only so much before the expansion limit of $F \to \infty$ (or D and $C \to 0$) is reached. Further inspection of (20a) will show that the flow angle downstream of the expansion fan corresponding to this limit is $\theta_e + \nu(Q_e) - \nu_{max}$. For some exit conditions (for example, normal exit at $\theta_e = 90°$) this angle will be positive, indicating that then the interface will surface ($D = 0$) along a line at this angle from the corner at x_e. Such a line would not mark a front, since the slope of the rising interface would be finite and continuous, but the plume flow there would then be detached from the shoreline and ambient water would lie at the surface shoreward of this line. This configuration is consistent with the isopycnal shapes at the inshore edge of the Connecticut plume in Fig. 2, and might be expected, since the Connecticut River exits roughly normal to the shore. It may also explain why no frontal boundary was ever observed on the inshore, downstream side of the Connecticut plume near the mouth (Garvine, 1974a and 1977), since existence of a front requires finite D in the plume just behind it.

Equation (20a) may be used to compute the flow properties in the near-shore uniform field. With these identified by "s" subscripts, we have $\theta_s = 0$ from the requirement that the flow parallel the shoreline, and thus from (20a)

$$\nu(Q_s) = \theta_e + \nu(Q_e) \tag{21}$$

Then (20b) may be used to find Q_s and (11), (12), and (13) to find C_s, D_s, and F_s. The downstream fan characteristic sets the upstream boundary of this region. This line has the inclination $\theta_s + \phi_s = \phi_s = \sin^{-1}(F_s^{-1})$. However, if the right-hand side of (21) exceeds ν_{max}, the flow will expand to the limit before reaching the shoreline, as discussed above, and no nearshore uniform field will exist.

The triangle bounding the exit uniform field has the vertices (0, 0), (x_e, 0), and (x_i, y_{fi}) shown in Fig. 5. The vertex (x_i, y_{fi}) is of particular physical significance, since it marks the *point of first arrival* at the front of an expansion wave from the downstream corner, and hence serves also as the origin of the first reflected characteristic.

Within the expansion fan flow properties may be readily computed from the relation for a single family wave. Following Milne-Thompson (1976, p. 611), we have for any given point (x, y) within the fan

$$\phi = \cot^{-1}[3^{1/2}\tan(3^{-1/2}\hat{\theta} + \varepsilon)] \tag{22a}$$

$$\theta = \theta_e + \phi_e - \hat{\theta} - \phi \tag{22b}$$

where

$$\hat{\theta} \equiv \theta_e + \phi_e - \tan^{-1}[y/(x - x_e)]$$

and

$$\varepsilon \equiv \cot^{-1}(3^{1/2}\tan\phi_e).$$

From ϕ all remaining properties may be computed.

5. Finite difference formulation

Downstream of the expansion fan and nearshore uniform field both families of characteristics are active in producing flow field changes; consequently no analytic solution exists there and a numerical or graphical solution must be sought instead. In this section I outline the finite difference scheme I used based on the method of characteristics.

The hyperbolic nature of the equations permits marching toward downstream away from a line along which the solution is known. Any such line will properly serve, provided it intersects all local characteristics of both families at a finite angle, i.e., it can nowhere be parallel to a characteristic. The resulting solution will then be unique within the *domain of the solution dependence*. If this line extends from the shoreline to the front, then the entire flow field downstream will be determined, provided inequality (18) is satisfied. Marching need not be in the x-direction; however, this type is the simplest and will be the only one I describe.

Fig. 6 shows the essentials of the scheme for an interior grid point, i.e., a point neither at the front nor the shoreline. The y-grid points have interval Δy, arbitrarily chosen. The solution is known at the grid points along x_m, either from the analytic solution valid for $x \le x_i$ (Fig. 4) or from the previous marching step for $x > x_i$. To find the solution at (x_{m+1}, y_n) the characteristic differential equations (7) must be applied in finite difference form along their corresponding characteristics which pass through the point. Since the difference scheme employed retained only first-order accuracy in Δx and Δy, these characteristics were approximated as straight lines with slopes given by (6) as computed at (x_m, y_m). To insure numerical stability the intercepts y_- and y_+ between these lines and the

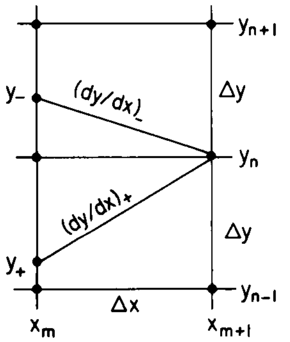

Fig. 6. Geometry of the finite difference scheme used for marching in the x-direction.

line $x = x_m$ must both fall within the interval y_{n-1} to y_{n+1}. This restriction amounts to satisfaction of the well known CFL condition for hyperbolic systems and may be stated compactly from the geometry of Fig. 6 as $K < 1$ where K is the Courant number

$$K \equiv \max\left[\left|\left(\frac{dy}{dx}\right)_+\right|, \left|\left(\frac{dy}{dx}\right)_-\right|\right]\Delta x/\Delta y \tag{23}$$

In the calculations I used $K = 0.8$. I computed values of Δx from (23) at each y-grid point along x_m and then selected the smallest of these for making the next marching step.

First order, finite difference equations for (7) may be written

$$2\theta_{m+1,n} = \theta_+ + \theta_- + (Q_+ - Q_-)/B$$

$$2Q_{m+1,n} = Q_+ + Q_- + B(\theta_- - \theta_+)$$

where

$$B \equiv Q_{m,n} \tan \phi_{m,n}$$

and the plus and minus subscripts refer to linearly interpolated values at y_+ and y_-. Application of (11), (12), (13), and (6c) using $Q_{m+1,n}$ then completes computation of the flow state at (x_{m+1}, y_n).

Boundary points along the shoreline ($y = y_s = 0$) must be computed differently. In place of the pair of characteristic differential equations (7), the two relations used in marching are $\theta_{s_{m+1}} = \theta_s = 0$ and the finite difference form of (7) for the minus characteristic family. Boundary values at the front where $y = y_f(x)$ must be computed differently, also. The next y coordinate of the front y_{fm+1} is computed by extrapolating the front downstream using the known frontal angle α_m. Two relations are then available to determine θ_{fm+1} and Q_{fm+1}. One is the finite difference form of (7) for the plus characteristic family. The other is the finite difference form for the relation between dQ_f and $d\theta_f$ obtained by differentiating the frontal jump conditions (16) and (17) and combining them with the differential of (11) to eliminate dC_f and $d\alpha$. These two difference equations may be applied simultaneously, of course, only if the plus characteristic intersects the front at x_{m+1} as a result of its greater inclination (Fig. 4b). However, this is guaranteed by satisfaction of inequality (18). Once Q_{fm+1} is determined, the other flow field variables are found, as for an interior point, and then α_{m+1} may be computed directly from (17).

6. Numerical results

Presentation of the computed plume flow fields centers upon a standard case for which results appear in Figs. 7 and 8. For this case zero entrainment was imposed at the front ($S_e = 0$) so that it represented a contact discontinuity ($\alpha = \theta_f$); the variations which entrainment imposes are discussed later. F_{a1} was set at unity, as for all other calculations. The ambient water velocity alongshore was set at $U_a = 1$ ($u_a = q^*$) and the outlet channel inclination at $\theta_e = 39°$ (thus, $\alpha_e = 39°$, also). Consequently, the outlet flow conditions were $Q_e = 1.48$, $C_e = 0.636$, $D_e = 0.405$, and $V_e =$

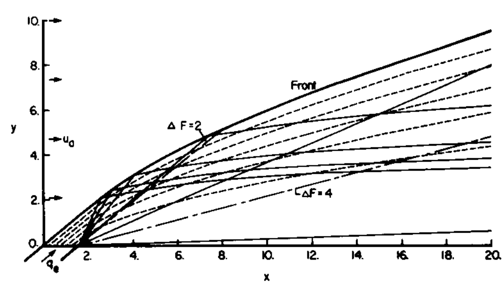

Fig. 7. Numerical results for the standard case. Ambient velocity u_a and exit velocity q_e have speeds proportional to their arrow lengths. Light, solid lines show selected characteristics, dashed lines show streamlines, and dash-dot lines show loci of constant shear Froude number ΔF. Distances shown along axes are normalized by the outlet channel width. The exit flow angle is $\theta_e = 39°$ and the normalized ambient velocity is $U_a = 1$.

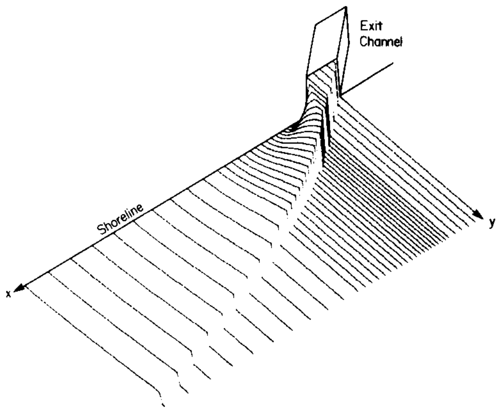

Fig. 8. Computer drawn isometric projection of the plume interface depth field (plotted upward) for the standard case (Fig. 7) as seen from offshore and above. The frontal boundary appears as a sharp drop to the x, y plane. Small irregularities in the offshore locations of the drop result from the discrete sampling used by the plotting algorithm.

$0.599wq^{*3}/g'$. These same outlet flow conditions were used for all other cases, the results of which are shown below.

Fig. 7 contains most of the flow field information. There are three principal physical features which appear clearly there and recur in all the other cases. The front bounds the flow offshore, no front is present inshore, and the flow itself simultaneously spreads laterally and turns toward the direction of the ambient flow alongshore. This third feature is one which would be required of any realistic model. If a plume exits into an open domain where a large scale ambient current is present, then the ultimate downstream state of the plume must include flow parallel to the ambient current. Furthermore, since the downstream dimension of the open domain is unlimited, the plume will spread downstream, in principle, until the limit $\theta \rightarrow 0$, $D \rightarrow 0$, and $Q \rightarrow 3^{1/2}$, is reached, corresponding to expansion of a compressible fluid into a vacuum.

Fig. 7 indicates the directions and relative magnitudes of the exit velocity q_e and ambient velocity u_a by means of arrows ($u_a/q_e = U_a/Q_e = 0.68$). Five interior streamlines are shown by dashed lines. These are separated by uniform intervals in the exit uniform field; consequently, farther downstream they continue to divide the plume into segments having the same volume flux, $V_e/6$ (see (19)). For this case both the front and the shoreline are streamlines also. Downstream of the exit uniform field most volume flux is concentrated offshore with the center streamline shifted toward the front away from its initial path along the plume's geometric centerline, $y_f(x)/2$.

This concentration of volume flux along the offshore side recurs in most of the other cases shown below. It can be explained as a consequence of plume depth variations rather than fluid speed changes. Ordinarily one would expect crowding of streamlines to reflect fluid speed changes. Here, however, little of this occurs. The normalized exit speed is $Q_e = 1.48$ and the maximum normalized speed is $q_m/q^* = 3^{1/2} \simeq 1.73$. Since plume water is always expanding (beyond the exit uniform field), all the fluid is accelerating; thus, all speeds are bounded by these values, restricting the maximum change in this case to only 17% of Q_e, too small even to justify drawing other plume velocity vectors in Fig. 7. Stronach (1981) has reported that changes in plume water speed are, indeed, small based on observations of drogue tracks in the Fraser River plume.

Instead, explanation lies in the plume depth variation across the streamlines. Fig. 8 shows a computer drawn isometric projection of the depth field D for the standard case as seen from offshore and above. For viewing convenience D is plotted positively upward. Since free surface elevation η and D are porportional, this field is also an image of the η field. In the outlet and in the exit uniform field the depth is maximum at $D_e = 0.405$. Thereafter it drops rapidly through the expansion fan, especially on the inshore side of it, but more slowly outward along the front. All offshore sections show D (or η) increasing monotonically offshore to a maximum at the front. Consequently, the volume flux, locally proportional to D, is concentrated on the offshore side of the plume.

A similar offshore concentration of plume depth was so often observed for the Connecticut River plume that I drew attention to it in discussing observations (Garvine, 1977, Figs. 13–16). I could offer no simple explanation then, but now one seems clear. To turn the streamlines toward alongshore from their initial angle θ_e a cross-stream pressure gradient is needed with higher pressure offshore. Thus η, and hence D, must increase offshore until the front is reached where D abruptly vanishes. This also illustrates how the front plays a vital dynamic role in connection with the entire plume flow field. As Fig. 8 suggests, the free surface slope, and hence the horizontal pressure gradient, is locally intense at the front and oppositely directed from that within the plume. This would lead to a sharp turning of the plume water toward the *offshore* direction at the front, roughly normal to the direction required of the ultimate downstream state. Hence, were it not for the presence of locally enhanced friction with the underlying ambient water which balances this pressure gradient at the front, the required downstream state could not be reached uniformly across the plume.

The internal wave field originating in the expansion fan is depicted in Fig. 7. Both the upstream and downstream fan characteristics, as defined in Fig. 5, are drawn as well as four other representative ones between them. The first three of these, as well as the upstream fan characteristic, reflect off the front as minus family waves within the domain shown ($x < 20$). The downstream fan characteristic nearly parallels the shore at $\phi_s = 2.0°$, since the nearshore uniform region inshore of it is close to the expansion limit with $Q_s = 1.73$, $D_s = 0.0034$, $C_s = 0.060$, and $F_s = 29.0$. The impact of these radiating expansion waves shows clearly in the rapid decline in D there shown in Fig. 8. By comparison, further expansion is much gentler in the downstream reach of the plume.

As outlined briefly above, in principle the flow would reach the downstream state of expansion in the limit $D \to 0$. However, based on physical processes not contained in the model, one would anticipate that at some distance downstream the fluid would become vulnerable to mean flow shear instabilities which would rapidly destroy the plume interface there. The critical bulk flow parameter is the shear Froude number

$$\Delta F \equiv |\mathbf{q} - u_a \mathbf{i}|/c$$

the internal Froude number based on the velocity shear across the interface. A value $\Delta F = 2$ corresponds to a bulk Richardson number of 1/4, and flows with $\Delta F < 2$ are stable. For some value of ΔF larger than 2 mean flow shear instability will rapidly lead to breaking internal waves and production of vigorous local, turbulent vertical exchange between plume and ambient water. The locus of points corresponding to this critical value of ΔF would then serve as a partial boundary to the plume near field, according to the definition of the near field in Section 1. This part of the near field boundary would be more diffuse than the frontal boundary, however. Precise critical values for ΔF depend on details of the mean flow density and velocity profiles, and so are not known for buoyant plumes at present. In Garvine (1977) seven estimates from observations for the Connecticut River plume near field correspond to values of ΔF which range from 1.1 to 2.9 with a mean value of 2.2. Thus, ΔF might reach as high as about 4. In Fig. 7 the lines corresponding to $\Delta F = 2$ and 4 are shown from the model computations. If we regard $\Delta F = 4$ as a provisional near field boundary, we see that for this case the near field would then be bounded downstream along a nearly straight line from the downstream corner.

By examining Figs. 9, 7 (the standard case), and 10, in that order, one may observe a sequence of plume flows with zero entrainment at the front for which θ_e increases monotonically while the outlet flow conditions (Q_e, C_e, D_e, F_e, and V_e) remain fixed. Thus, since $\alpha_e = \theta_e$ for each, U_a decreases monotonically by (17). Values for θ_e and U_a appear in the figure captions.

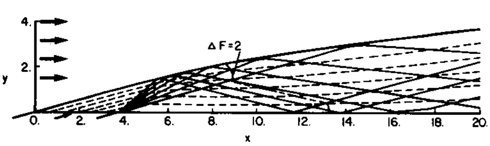

Fig. 9. As in Fig. 7, except $\theta_e = 15.3°$ and $U_a = 2.41$. Note the clear presence of the nearshore uniform region (Fig. 5) where $\theta = 0$ in the isosceles triangle between x about 4 and 12.

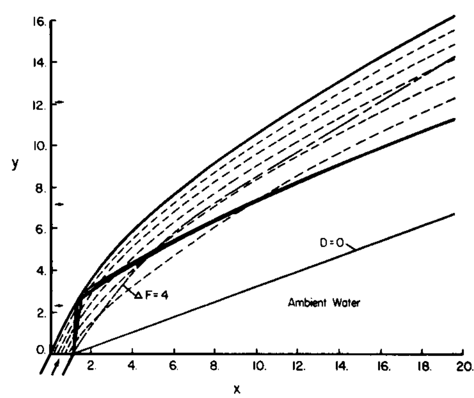

Fig. 10. As in Fig. 7, except $\theta_e = 63°$ and $U_a = 0.714$. The line $D = 0$ is inclined at 20°.

A number of general trends are clear. As θ_e increases, the front becomes more steeply inclined so that the plume reaches farther offshore. This trend is consistent with the two limiting cases for the exit uniform field, U_a large and small. As discussed in Section 3, for larger U_a the front is confined closer to shore, while for smaller U_a it penetrates farther outward, but in the limit for $U_a \to 0$ the plume then approaches the wisp of width w moving offshore along a straight line. Elements of this latter structure are visible in Fig. 10 where we see almost all of the streamlines near the front.

The plume does not widen as rapidly as its front moves offshore, however, since its ultimate inshore edge becomes the line $D = 0$ in Fig. 10 where the expansion limit is reached, leaving ambient water at the surface further inshore. As the outlet angles become large the streamlines crowd more and more toward the offshore side of the plume near the front. In Fig. 10, the outermost pair of streamlines are separated by only about a tenth the distance between the innermost pair (the most inshore dashed line and the line $D = 0$), while between each pair flows the same volume flux, $V_e/6$; thus, the plume depth is quite small between the innermost pair. Another general trend is the offshore migration of the line $\Delta F = 4$ with increasing θ_e. This line is not even present in Fig. 9, but by Fig. 10 it remains within a distance of the front not much larger than the outlet channel width. If this line were interpreted as the inshore near field boundary, then the widest plume is actually that of Fig. 7.

The geometry of the reflected expansion fan characteristics also displays a general trend. For the shallower outlet angles of Figs. 9 and 7 these diverge in passing downstream, while for the steeper outlet angle of Fig. 10 they converge and nearly coalesce at about $x = 20$. This implies the formation of an internal hydraulic jump interior to the plume beginning at the convergence and continuing downstream, eventually to intersect the line $D = 0$. In nature this interior jump is unlikely to occur because, as the figure shows, it would lie in a region of very large ΔF where mean shear flow instability would likely have destroyed the plume near field structure some distance upstream.

All of the above cases have specified zero frontal entrainment ($S_e = 0$) for simplicity of interpretation. Fig. 11 shows results for entraining fronts. Fig. 11b reproduces the standard case to provide a benchmark for zero entrainment. The outlet flow conditions (C_e, etc.) are again the same and the exit flow angle is kept at $\theta_e = 39°$. Fig. 11a corresponds to upward entrainment in the frontal zone ($S_e = +1$) with turbulent exchange parameter $\beta = 0.2$, while Figs. 11c and d correspond to downward entrainment ($S_e = -1$) with $\beta = 0.2$ and 0.4, respectively. For small-scale surface fronts such as these, the weight of evidence from field observations, laboratory experiments, and frontal zone models strongly supports downward, not upward, entrainment. Nevertheless, cases for both

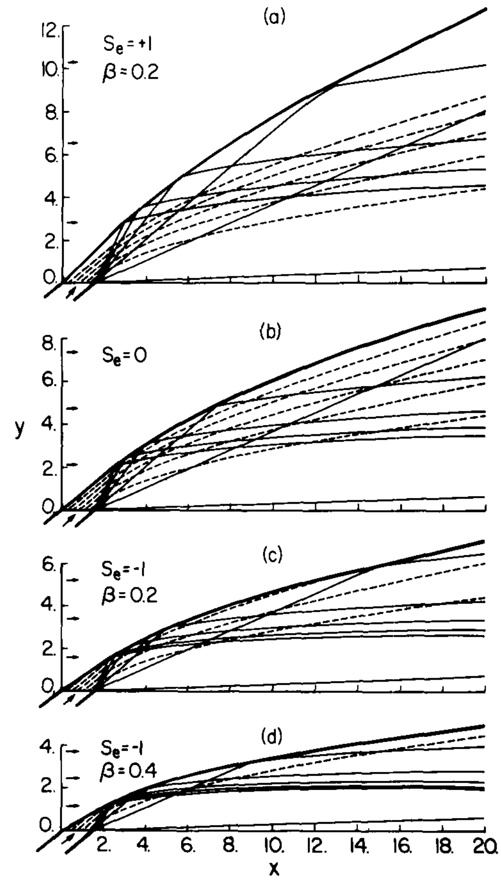

Fig. 11. Flow field as in Fig. 7 but with entrainment at the front. (a) Upward entrainment with $\beta = 0.2$. $U_a = 0.915$ and $\alpha_e = 44°$. (b) As in Fig. 7. Zero entrainment. $U_a = 1$ and $\alpha_e = 39°$. (c) Downward entrainment with $\beta = 0.2$. $U_a = 1.14$ and $\alpha_e = 34°$. (d) Downward entrainment with $\beta = 0.4$. $U_a = 1.31$ and $\alpha_e = 29°$.

types are displayed here to assess more fully the effect of frontal mass entrainment on the plume structure.

The major effect of entrainment is seen to be its control of the local angle between the front and the plume streamline angle behind the front, i.e., $\alpha - \theta_f$. For upward entrainment this angle is necessarily positive (see (16)), since in the frontal zone ambient water crosses the interface to enter and mix with plume water. (The effect this would have on the plume water density is neglected in this model where g' = constant.) Since θ_e is the same for all the cases, this one has the largest frontal inclination with $\alpha_e = 44°$, and, hence, has the widest plume. For downward entrainment $\alpha - \theta_f$ is necessarily negative; hence, in Figs. 11c and d we see most of the plume streamlines terminating at the front where plume water is being entrained and mixed downward into the local ambient water. For greater turbulent exchange (large β) this happens more rapidly. Concurrently, the frontal angles are smaller with $\alpha_e = 34°$ and $29°$. Clearly downward entrainment would lead to more rapid mixing of plume and ambient water and to plume near fields more limited in both lateral and downstream extent.

7. Concluding remarks

The present model permits examination of the simultaneous action in the near field of a buoyant surface plume of gravitational spreading, frontal boundaries, and alongshore motion of ambient water. The model dynamics reflect the action of inviscid, nonlinear internal waves in the plume body and turbulent exchange of mass and momentum in the frontal zone.

The model shows a number of prominent physical characteristics. Frontal boundaries are found only on the offshore side of the plume where the ambient current component normal to the front confines plume spreading. As the plume spreads beyond the outlet channel it simultaneously turns downstream toward alignment with the ambient current. This simultaneous action is made possible by the dynamics of the frontal boundary where the intense horizontal pressure gradient is principally balanced by interfacial friction. The turning of the plume downstream is forced by the pressure field which features higher pressure offshore near the front which, in turn, requires that the plume interface be deeper there. Since the plume water speed can change relatively little, this leads to concentration of the plume volume flux along its offshore side near the front. All of these features are intensified by increased outlet channel inclination angle to the shoreline, or, equivalently, by decreased ambient current, since greater turning of the flow is then required. However, the initial turning angle is limited to a maximum of less than 66°, since then the associated flow expansion and opening up of flow streamlines brings the interface to the free surface. Thus, outlet channel inclincations greater than 66° produce plumes which are separated from the shoreline by ambient water. In nature, however, mean flow shear instability will likely restrict the inshore plume boundary to a line further offshore, along which the shear Froude number reaches some critical value greater than 2.

Most of the plume spreading or expansion occurs in the initial passage of plume water through the expansion fan of internal wave fronts centered at the downstream corner of the outlet channel. The flow in the exit uniform field and in the expansion fan can be determined by analytic computation. Consequently, recourse to more complicated numerical solutions is necessary only for determining the flow field farther downstream.

Mass entrainment in the frontal zone affects the shape and structure of the entire plume field. For downward entrainment at the front the plume streamlines intersect the front leading to plumes which are more confined and which mix more rapidly with ambient water.

The model results explain many of the observed qualitative features of the Connecticut River plume in Long Island Sound. Several of these were previously unaccounted for, such as the offshore deepening of the plume and the failure of frontal boundaries to form on the inshore side. Direct quantitative comparisons with such plumes, however, will require further model development to account for earth rotation and time dependence.

8. Acknowledgments

I am grateful for the support of this work by the National Science Foundation through Grant No. OCE-7821318. Dr John P. Ianniello provided many comments for improving the manuscript.

REFERENCES

Abbott, M. B. 1961. On the spreading of one fluid over another. *La Houille Blanche* 622–628 and 827–846.

Courant, R. and Friedrichs, K. O. 1976. *Supersonic Flow and Shock Waves*. New York: Interscience Publishers, Inc.

Ferri, A. 1954. The method of characteristics. Section G. In *General Theory of High Speed Aerodynamics* (ed.) W. R. Sears. Vol. VI, *High Speed Aerodynamics and Jet Propulsion*. Princeton: Princeton Univ. Press, 583–669.

Garvine, R. W. 1974a. Physical features of the Connecticut River outflow during high discharge. *J. Geophys. Res. 79*, 831–846.

Garvine, R. W. 1974b. Dynamics of small-scale oceanic fronts, *J. Phys. Oceanogr. 4*, 557–569.

Garvine, R. W. 1977. Observations of the motion field of the Connecticut River plume. *J. Geophys. Res. 82*, 441–454.

Garvine, R. W. 1981. Frontal jump conditions for models of shallow, buoyant surface layer dynamics. *Tellus 33*, 301–312.

Garvine, R. W. and Monk, J. D. 1974. Frontal structure of a river plume. *J. Geophys. Res. 79*, 2251–2259.

Jirka, G. 1980. Two-dimensional density current from continuous source in stratified crossflow. *Proc. 2nd Int. Symp. on Stratified Flows 2*, 860–870.

Kao, T. W., Park, C. and Pao, H.-P. 1977. Buoyant surface discharge and small-scale oceanic fronts: a numerical study. *J. Geophys. Res. 82*, 1747–1766.

Liepmann, H. W. and Roshko, A. 1957. *Elements of Gas Dynamics*. New York: John Wiley & Sons, Inc.

Milne-Thompson, L. M. 1976. *Theoretical Hydrodynamics*, London: the MacMillan Press, Ltd.

Stoker, J. J. 1957. *Water Waves*. New York: Interscience Publishers, Inc.

Stronach, J. A. 1981. The Fraser River plume, Strait of Georgia. *Ocean Management. 6*, 201–221.